

Sporadic ALS has compartment-specific aberrant exon splicing and altered cell–matrix adhesion biology

Stuart J. Rabin¹, Jae Mun ‘Hugo’ Kim¹, Michael Baughn¹, Ryan T. Libby¹, Young Joo Kim^{1,†}, Yuxin Fan^{1,‡}, Randell T. Libby², Albert La Spada^{2,¶}, Brad Stone¹ and John Ravits^{1,3,*}

¹Translational Research Program, Benaroya Research Institute at Virginia Mason, Seattle, WA 98101, USA, ²Center for Neurogenetics & Neurotherapeutics, University of Washington, Seattle, WA 98195, USA and ³Section of Neurology, Virginia Mason Medical Center, Seattle, WA 98101, USA

Received August 7, 2009; Revised October 9, 2009; Accepted October 26, 2009

Amyotrophic lateral sclerosis (ALS) is a fatal neurodegenerative disease characterized by progressive weakness from loss of motor neurons. The fundamental pathogenic mechanisms are unknown and recent evidence is implicating a significant role for abnormal exon splicing and RNA processing. Using new comprehensive genomic technologies, we studied exon splicing directly in 12 sporadic ALS and 10 control lumbar spinal cords acquired by a rapid autopsy system that processed nervous systems specifically for genomic studies. ALS patients had rostral onset and caudally advancing disease and abundant residual motor neurons in this region. We created two RNA pools, one from motor neurons collected by laser capture microdissection and one from the surrounding anterior horns. From each, we isolated RNA, amplified mRNA, profiled whole-genome exon splicing, and applied advanced bioinformatics. We employed rigorous quality control measures at all steps and validated findings by qPCR. In the motor neuron enriched mRNA pool, we found two distinct cohorts of mRNA signals, most of which were up-regulated: 148 differentially expressed genes ($P \leq 10^{-3}$) and 411 aberrantly spliced genes ($P \leq 10^{-5}$). The aberrantly spliced genes were highly enriched in cell adhesion ($P \leq 10^{-57}$), especially cell–matrix as opposed to cell–cell adhesion. Most of the enriching genes encode transmembrane or secreted as opposed to nuclear or cytoplasmic proteins. The differentially expressed genes were not biologically enriched. In the anterior horn enriched mRNA pool, we could not clearly identify mRNA signals or biological enrichment. These findings, perturbed and up-regulated cell–matrix adhesion, suggest possible mechanisms for the contiguously progressive nature of motor neuron degeneration. Data deposition: GeneChip raw data (CEL-files) have been deposited for public access in the Gene Expression Omnibus (GEO), www.ncbi.nlm.nih.gov/geo, accession number GSE18920.

INTRODUCTION

Amyotrophic lateral sclerosis (ALS) is an adult-onset idiopathic fatal neurodegenerative disease caused by highly selec-

tive loss of motor neurons (1). The main clinical features are insidious onset of upper and lower motor neuron degeneration and relatively linear progression over time. The main neuropathological features are loss of motor neurons. The age at

*To whom correspondence should be addressed at: Translational Research Program, Benaroya Research Institute at Virginia Mason, 1201 Ninth Avenue, Seattle, WA 98101, USA. Tel: +1 2063411944; Fax: +1 2062237543; Email: jravits@benaroyaresearch.org

[†]Present address: Programs in Biomedical and Biological Sciences, University of Southern California, Los Angeles, CA 90089, USA.

[‡]Present address: John Welsh Cardiovascular Diagnostic Laboratory, Department of Pediatrics (Cardiology), Texas Children’s Hospital, Baylor College of Medicine, Houston, TX 77030, USA.

[¶]Present address: Departments of Pediatrics and Cellular & Molecular Medicine, Rady’s Children Hospital, University of California, San Diego 2123, USA.

onset is usually over 25 years and incidence increases slightly with age. The overall incidence of ALS is 2–3 per 100 000 and the prevalence is 6–10 per 100 000. Ninety to 95% of cases are sporadic (SALS) and 5–10% of cases are familial (FALS), for which ~30% of the mutations have been identified to date. There are no effective treatments and death occurs in 90% of patients within 3–5 years. The mechanisms for the highly selective degeneration are unknown (2) and it is increasingly thought that non-neuronal cells are involved in the process (3,4). It is now recognized that close associations between ALS and frontotemporal lobar dementia with ubiquitin and TDP-43 positive immunoreactivity exist at the clinical, pathological, and molecular levels (5).

Alternative exon splicing is now believed to be one of the major factors determining the complexity and functionality of the eukaryotic genome (6–8). It is one of the main mechanisms of gene and cell regulation, modulates the properties of encoded proteins by regulating expression and adding and deleting functional domains and likely involves most genes. The control of exon splicing involves regulatory proteins binding to a variety of sites on transcripts such as exon splicing enhancers that bind SR proteins, polypyrimidine tracts, and splice motifs. The primary mediator of splicing is the spliceosome, composed of over 100 splicing factors including proteins, RNA and small nuclear ribonucleoproteins, which associate with pre-mRNA to mediate intron excision and exon ligation (9). Abnormal splicing can result in disease and the list of diseases attributed to this continues to grow (10). Appreciation of the significance of exon splicing in the genome has grown recently due to better analytic techniques (11) and is now entering an even more rapid growth phase with technology to perform deep sequencing (12).

There is increasing evidence that implicates abnormalities of RNA processing and exon splicing in ALS pathogenesis (13). TDP-43, a protein that has known functions in RNA processing and regulation of exon splicing, mislocalizes from the nucleus to the cytoplasm in SALS, suggesting its nuclear pre-mRNA functions are fundamentally compromised (14–16). Mutations in the TARDBP gene encoding the TDP-43 protein are found in both FALS and SALS, indicating its role can be primary (17–19). There is strong evidence that the toxic property resides in the C-terminal fragments, an architecture that would likely compromise nuclear functions, including exon splicing. Recently, the FUS/TLS gene has been identified in FALS by virtue of its function in RNA processing (20,21). Among the other genes identified to date in ALS as well other motor neuron degenerative disorders, there is over-representation of genes encoding proteins that are involved in RNA processing; these include: SETX, SMN, GARS, ATXN7, IGHMBP2 and ANG (22). A newly reported association has been identified between ALS and variants of a component of RNA polymerase II, elongator protein 3 (23). And spinal muscular atrophy (SMA), the most common motor neuron disease in childhood, is caused by homozygous loss of the SMN1 gene, which plays key roles in exon splicing (24).

Motor phenotypes of ALS indicate that underlying motor neuron degeneration is a focal process that progresses contiguously along neuronal anatomy (25). Neuropathological stages can be defined in relation to the site of onset, advanced in the region of onset and progressively less radially away (26). This

creates opportunity for functional genomics analysis, as genomic signals can be isolated from regions in early to intermediate stages of degeneration and profiled using newly available laser and microchip technologies (27,28). To pursue this, we created a tissue repository specifically for simultaneous genomic and structural studies, used histopathology to identify suitable neuron-rich regions, validated RNA quality and profiled exon and gene expression in motor neurons and its anterior horn microenvironment. Using powerful bioinformatics approaches, we identified biological signals in motor neuron enriched mRNA pools that appear to be perturbed in SALS, the strongest of which is abnormal exon splicing, especially in cell-matrix adhesion genes. The pathogenesis of SALS remains elusive and mainly pursued by way of laboratory models of genetic disease—our findings identify important new aspects directly in human sporadic disease.

RESULTS

Special processing of CNS coupled with laser capture microdissection permits collection and selective enrichment of relevant cellular compartments for genomic analysis

Major challenges facing genomic analysis of human degenerative disorders of the CNS are precise localization and isolation of the degenerating compartment and the proper acquisition of materials. As SALS disease typically exhibits a focal onset and subsequent spread (25,26), patients whose disease began in bulbar and arm regions have caudally advancing disease and often have lumbar regions in relatively early stages of degeneration at the time of death. To exploit this, we developed an on-call autopsy system and rapidly harvested their nervous systems, usually completed within 6 h of death, and specifically processed them for downstream genomic and structural studies. We used histopathology to confirm that the lumbar regions distal to the site of onset had early or intermediate stage of disease pathology with abundant residual motor neurons and that they contained TDP-43 cytoplasmic deposits characteristic of SALS. Based upon this analysis and upon analysis of RNA quality as discussed below, we then chose nervous systems from the frozen inventory and collected from them motor neurons by laser capture microdissection in SALS ($n = 12$) and controls ($n = 10$) (Table 1 and Fig. 1A). After we had completed collection of motor neurons by microdissection, we collected the remaining anterior horn region to create a second sample set, reasoning that this might be important for understanding disease pathogenesis given the strong evidence for non-autonomous degeneration in ALS (3,4). For standardization, we studied lumbar regions in all cases, disease and control.

RNA and microarray quality are high

The success of genomic profiling depends upon both RNA and microarray quality. To ensure RNA quality, we used digital micro-electrophoresis and performed extensive validation of RNA quality (Supplementary Material S1). We found that our human RNA quality was high, RNA quality was sufficiently preserved through the steps of microdissection, and

Table 1. Demographic details

Primary diagnosis	CNS ID number	Age	Gender	Site of onset	Disease course (years)	PMI (h)
SALS	14	73	Female	Bulbar	1.5	6
SALS	16	61	Male	Arm	2.5	3.5
SALS	17	55	Male	Arm	2	3
SALS	18	80	Female	Bulbar	2	4
SALS	27	74	Male	Bulbar	3.25	4
SALS	33	54	Male	Arm	6.5	5
SALS	34	81	Female	Bulbar	1	3.5
SALS	35	74	Female	Bulbar	5.75	5
SALS	60	58	Female	Bulbar	3	3
SALS	63	68	Male	Arm	2.5	5
SALS	64	47	Male	Arm	3	6.5
SALS	68	72	Female	Leg	1.5	4
Control	10	78	Male	NA	NA	2.5
Control	19	80	Female	NA	NA	2.5
Control	26	49	Male	NA	NA	4
Control	39	77	Male	NA	NA	2
Control	42	61	Male	NA	NA	6
Control	44	80	Female	NA	NA	5
Control	55	71	Male	NA	NA	13
Control	59	73	Male	NA	NA	8
Control	65	82	Male	NA	NA	4
Control	67	77	Male	NA	NA	4

mRNA signals amplified to yield quantities and qualities necessary for microarray analysis (Fig. 1B). When RNA was optimal, we proceeded to label it, hybridize it to exon arrays, and process the arrays to CEL files. To ensure microarray quality, we examined CEL files in multiple ways (see Materials and Methods) and we found they were uniformly high (Supplementary Material S1). We always processed equal numbers of SALS and controls together to minimize batch effects and upon completion of the studies, we measured batch effects and they were minimal (data not shown), indicating evenness of acquired data between disease and control. We compared both RNA and microarray quality with our analogous experiments in ALS1 G93A transgenic mice using 3' gene expression arrays, which were performed under ideal laboratory-controlled conditions, and found they were comparable (RNA quality is shown in Figure 1B and CEL file data are not shown). Thus, we were reassured of the high quality and reliability of the signals we acquired with our approach.

Genomic analysis identifies differentially expressed gene signals in the motor neuron enriched mRNA pool

We next looked at differential gene expression. One of the main challenges of doing this is ascertaining significance when there are multiple tests and uncertain levels of noise. To determine noise levels in our data, we created sham test groups by permuting CEL file test categories and computing differential gene expression 10 times and then compared differential gene expression in our true data with the sham data (see Materials and Methods). In the motor neuron enriched mRNA pool, we found robust differential expression and readily definable noise levels: we estimate a data-specific 5% noise threshold of $P \approx 10^{-3}$ and at this level of significance, there are 148 differentially expressed genes in the true data set and an average of six genes (range 2–12) in

the permuted data sets (Fig. 2A, Table 2 and Supplementary Material S2). Most of the differentially expressed genes are up-regulated rather than down-regulated—for a fold change ≥ 1.5 , 71 genes are up-regulated and 14 genes are down-regulated—suggesting increasing rather than decreasing molecular activity in the motor neuron enriched mRNA pool.

Exon splicing is significantly aberrant in the motor neuron enriched mRNA pool and is distinct from and more pronounced than differential gene expression

We next looked at exon splicing. To determine aberrant exon splicing, we used an ANOVA-based analysis that generates *P*-values indicating the probability of aberrant splicing occurring in a particular gene. The ANOVA-based analysis separates out many variables, most importantly overall gene expression levels. As with differential gene expression, one of the main challenges is ascertaining significance with multiple tests and uncertain levels of noise and we employed the same strategy of permutation analysis that we used in analyzing differential gene expression. In the motor neuron enriched mRNA pool, we again found robust signals and readily definable noise levels: we estimate a data-specific 5% noise threshold of $P \approx 10^{-5}$ and at this level of significance, there are 411 aberrantly spliced genes in the true data set and an average of 21 genes (range 5–51) in the permuted data sets (Fig. 2B, Table 2 and Supplementary Material S2). Comparing aberrantly spliced genes to differentially expressed genes, we see a nearly 3-fold greater number (411 versus 148) using our data-specific noise levels to define the respective cohorts. Analysis of these cohorts indicates only 29 genes overlap—7% of the 411 aberrantly spliced genes and 21% of the 148 differentially expressed genes (Fig. 2E)—thus showing that the cohorts of genes are distinct from each other. The greater numbers of aberrantly spliced genes than differentially expressed genes cannot be attributed to the greater degree of multiple testing since this and other methods of analysis we used correct for this. As with the differential gene expression, most of the aberrantly spliced genes were up-regulated rather than down-regulated. To examine the architecture of aberrant splicing in these genes, we classified splicing abnormalities in the top 100 genes and found that 56% had changes in internal exons, 51% in 5' regions, 36% in 3' regions and 42% in multiple locations (both internal and terminal) (data not shown).

The aberrantly spliced genes but not the differentially expressed genes in the motor neuron enriched mRNA pool are biologically enriched

One of the main challenges of microarray analysis is ascertaining biological importance of identified genes—statistical significance does not equate to biological significance. Multiple approaches have been designed to meet these challenges (29,30) and one approach is by scoring enrichment from the Gene Ontology (GO) (www.geneontology.org) by way of a χ^2 test (see Materials and Methods). Accordingly, we calculated this for both differentially expressed genes and for aberrantly spliced genes. Enrichment analyses often can be difficult to interpret and *P*-values deceptively low and thus in order to

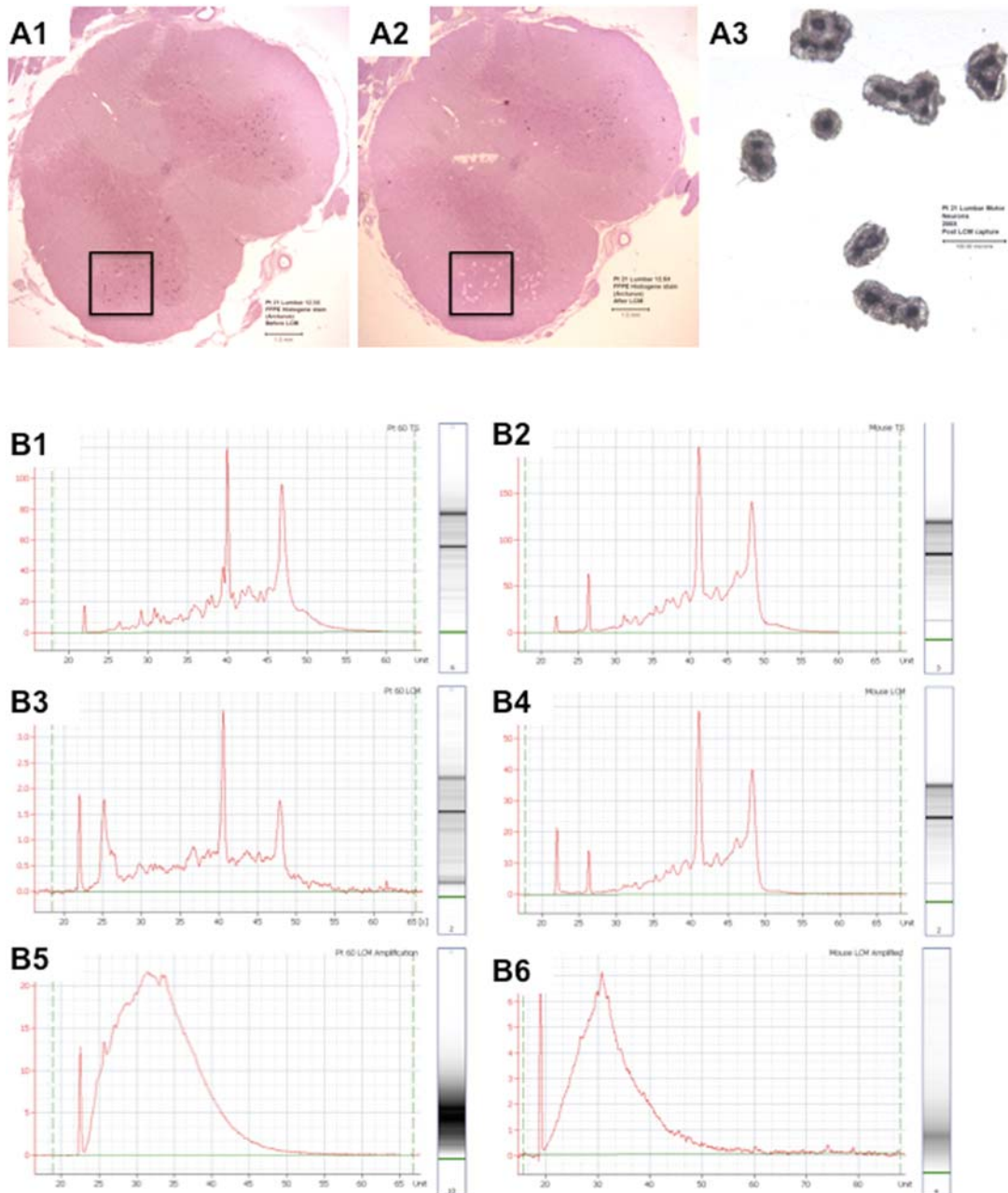


Figure 1. Laser capture microdissection (LCM) permits collection of high quality RNA from SALS motor neurons. (A): (A1) This is a low-power transverse view of SALS lumbar spinal cord stained with H&E before LCM. The rectangle indicates the anterior horn. Note the relative abundance of residual lumbar motor neurons (purple spots) in this nervous system where disease onset was in arm and respiratory muscles. (A2) Same, after LCM—the small white blanks are where motor neurons were microdissected. Note the specificity that is achieved within the complex cytoarchitecture of the spinal cord. (A3) This is a mid-power view of motor neurons captured and adhering to a thermoplastic polymer film on an LCM cap. The cap fits into a microtube for RNA isolation. [Scale bars are 1 mm in (A1) and (A2) and 100 μm in (A3)]. (B) These are electropherograms (left side of each panel) and digital gels (right side of each panel) generated by digital micro-electrophoresis that is used to assess RNA quality. The column on the left (B1, B3 and B5) is from a SALS nervous system and the column on the right (B2, B4 and B6) is from a SOD1 G93A ALS1 transgenic mouse for comparison. The top row (B1 and B2) shows total RNA before processing by laser capture microdissection (LCM). The middle row (B3 and B4) shows total RNA of motor neurons after isolation by LCM. The bottom row (B5 and B6) shows messenger RNA from the laser captured motor neurons after amplification. The similarities in these tracings illustrate the high quality of RNAs generated from SALS patient materials.

understand our results, we also calculated enrichment in each of the 10 permuted data sets using a comparable number of genes. Analysis of differentially expressed genes in the motor neuron enriched mRNA pool did not reveal clearly definable biological enrichment above noise levels (Fig. 2C). But enrichment analy-

sis of the aberrantly spliced gene cohort, in contrast, revealed robust enrichment above noise levels: we estimate a data-specific 5% noise level threshold of $P \approx 10^{-20}$ and at this level of significance, there are 33 pathways in our true data and an average of 1.6 pathways (range 0–4) in our permuted

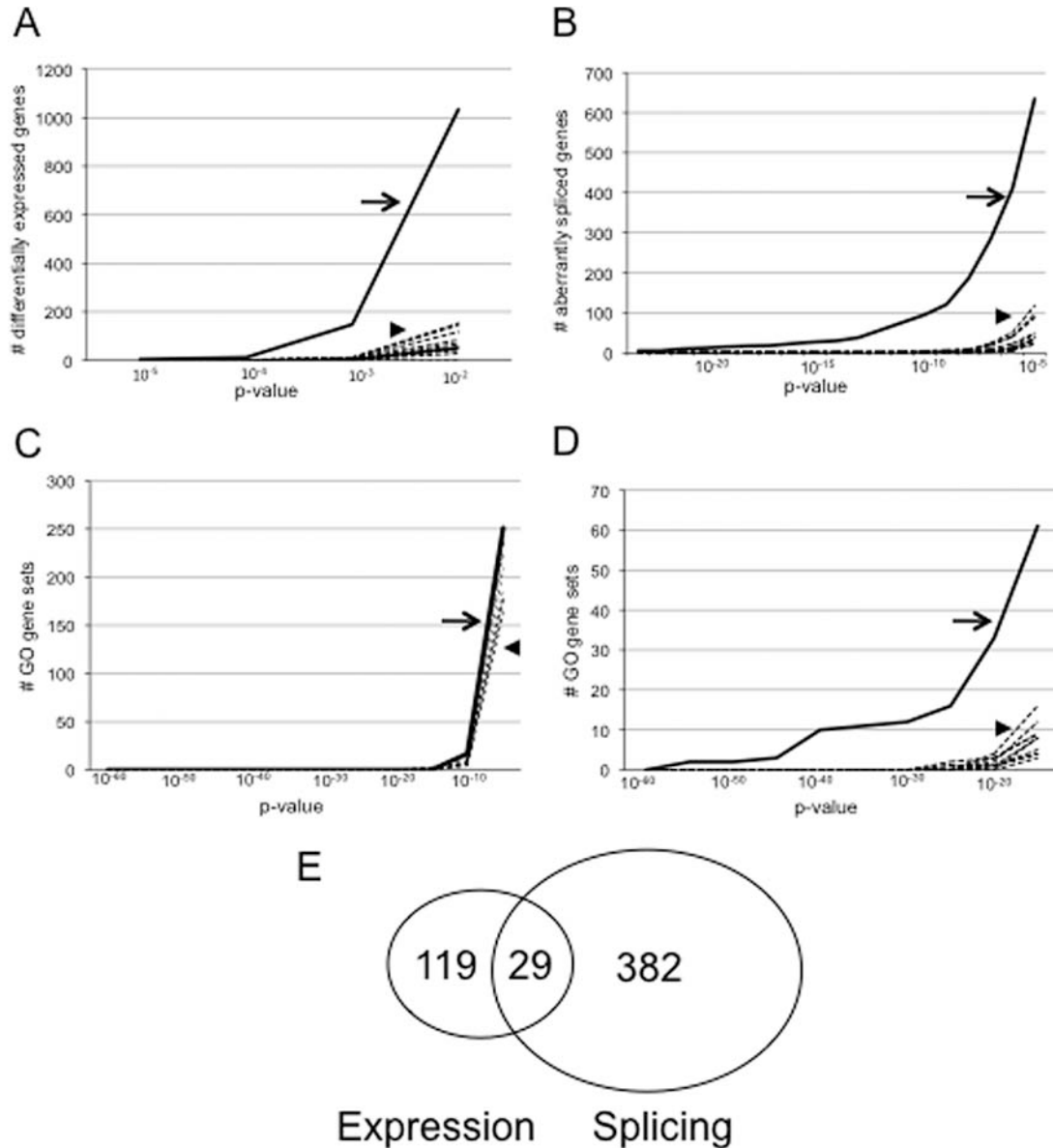


Figure 2. Microarray analysis robustly identifies disease-associated signals in the SALS motor neuron enriched mRNA pool. **(A)** This graph shows the cumulative numbers of differentially expressed genes as a function of P -values. In this and in the other graphs, the solid line (arrow) shows the true comparison between SALS and control and the dashed lines (arrowhead) show sham comparisons of randomly permuted groups and indicate the noise levels in the data. Highly distinct differential gene expression is identified. **(B)** This graph shows the cumulative numbers of aberrantly spliced genes as a function of P -values. Note not only that significant aberrant gene splicing is identified, but also that the degree of abnormality is greater than seen with differential gene expression. **(C)** This graph shows cumulative numbers of Gene Ontology gene sets that enrich the differentially expressed genes identified in **(A)** as a function of P -value. There is no apparent biological enrichment of the differentially expressed genes. **(D)** This graph shows cumulative numbers of Gene Ontology gene sets that enrich the aberrantly spliced genes identified in **(C)** as a function of P -value. By comparison to differential gene expression, the aberrantly spliced genes are robustly enriched biologically. **(E)** Venn diagram comparing differentially expressed and aberrantly spliced genes in the SALS motor neuron enriched RNA pools. Note that the two cohorts of genes are distinctive and have only slight overlap.

data (Fig. 2D and Supplementary Material S2). Some gene sets have enrichment P -values $< 10^{-57}$.

The specific enrichments that we identified in the motor neuron enriched mRNA pool are predominately related to cell adhesion and extracellular matrix (ECM) biology (Table 3 and Supplementary Material S2). Transmembrane receptor protein tyrosine kinase activity, vascular endothelial growth factor receptor activity and regulation of cell motility

were also identified (Table 3 and Supplementary Material S2). While the 33 gene sets with $P \leq 10^{-20}$ contained a total number of 355 genes, many genes appeared redundantly in the gene sets and only 111 of these were unique. Of these, 57 specifically relate to cell adhesion and related functions (Fig. 3). In the sub-categories of cell adhesion, genes associated with cell-matrix adhesion and cell-substrate adhesion were far more abundant than those associated with cell-cell

Table 2. Top 25 aberrantly spliced and top 25 differentially expressed genes

Gene symbol	Gene name	RefSeq	Alt. splice P-value	Differential expression P-value	Fold-change (A versus C)	# Markers (exons)
ABCA8	ATP-binding cassette, sub-family A (ABC1), member 8	NM_007168	2.84E-17	0.0147702	2.07853	37
ACADVL	Acyl-Coenzyme A dehydrogenase, very long chain	NM_000018	0.07572	9.62E-05	-1.36709	20
AGTRL1	Angiotensin II receptor-like 1	NM_005161	0.00280309	0.000100449	2.80667	6
AQP4	Aquaporin 4	NM_001650	1.35E-27	1.21E-06	3.17926	13
ASPA	Aspartoacylase (Canavan disease)	NM_000049	0.199691	0.000120487	2.94572	6
C1orf198	Chromosome 1 open reading frame 198	AK096166	2.66E-16	0.00111187	1.7294	17
C21orf33	Chromosome 21 open reading frame 33	NM_004649	0.0218155	0.00010392	-1.30992	10
C3	Complement component 3	NM_000064	1.89E-23	0.00107972	2.39112	43
C4A	Complement component 4A (Rodgers blood group)	NM_007293	1.88E-31	0.000487554	2.3395	48
CENTD1	Centaurin, delta 1	NM_015230	9.18E-08	8.68E-05	1.86511	37
COG5	Component of oligomeric golgi complex 5	NM_006348	1.79E-05	0.000102532	1.63965	28
COL1A2	Collagen, type I, alpha 2	NM_000089	2.02E-24	0.0319974	1.44001	47
COL6A3	ollagen, type VI, Calpha 3	NM_004369	3.34E-20	0.0945555	1.36456	45
CPVL	Carboxypeptidase, vitellogenic-like	NM_019029	3.89E-11	6.99E-06	2.06165	17
CXCL16	Chemokine (C-X-C motif) ligand 16	NM_022059	0.00011424	2.01E-05	1.99739	10
DST	Dystonin	NM_183380	9.73E-24	0.323111	1.0925	125
EDNRB	Endothelin receptor type B	NM_000115	2.64E-19	1.64E-05	3.01733	17
ELAVL3	ELAV (embryonic lethal, abnormal vision, Drosophila)-like	NM_032281	1.12E-05	0.000109817	-2.14778	18
EXOSC6	Exosome component 6	NM_058219	0.804989	0.000105887	-1.21483	7
FAM46C	Family with sequence similarity 46, member C	NM_017709	6.43E-08	0.000117789	2.4746	6
FLJ21963	FLJ21963 protein	NM_024560	2.64E-12	2.35E-05	3.01776	17
FLJ44874	FLJ44874 protein	AK126822	0.597731	1.44E-07	-1.46746	3
FLNC	Filamin C, gamma (actin-binding protein 280)	NM_001458	2.80E-16	0.289023	1.0877	48
FN1	Fibronectin 1	NM_212482	2.24E-21	0.0133788	2.50828	63
HIF3A	Hypoxia inducible factor 3, alpha subunit	NM_022462	6.33E-16	0.0968477	1.24509	27
HLA-B	Major histocompatibility complex, class I, B	NM_005514	0.011742	0.000145132	2.07808	3
HLA-DMB	Major histocompatibility complex, class II, DM beta	NM_002118	0.00334092	0.000122339	2.64162	3
HLA-DRA	Major histocompatibility complex, class II, DR alpha	NM_019111	0.0176529	9.96E-06	3.75813	9
INPP5D	Inositol polyphosphate-5-phosphatase, 145 kDa	NM_005541	2.28E-15	0.00485491	1.54023	25
KIAA0644	KIAA0644 gene product	NM_014817	5.30E-18	0.0764209	1.16279	15
KRT73	Keratin 73	NM_175068	0.156092	6.78E-05	-1.35392	9
LRP1	Low-density lipoprotein-related protein 1 (alpha-2-macroglo	NM_002332	2.68E-19	0.0219457	1.28675	105
MACF1	Microtubule-actin cross-linking factor 1	NM_012090	7.85E-22	0.00408213	1.24486	115
MYBPC1	Myosin binding protein C, slow type	NM_002465	1.90E-21	0.00967833	1.31138	31
OR2W3	Olfactory receptor, family 2, subfamily W, member 3	NM_001001957	0.602669	0.000100305	-1.45266	13
OR5AS1	Olfactory receptor, family 5, subfamily AS, member 1	NM_001001921	0.548751	0.000141626	-1.3982	3
PADI2	Peptidyl arginine deiminase, type II	NM_007365	9.72E-14	0.000114651	1.6916	18
PARP9	Poly (ADP-ribose) polymerase family, member 9	NM_031458	0.606104	2.15E-05	3.48026	3
PCDHGC5	Protocadherin gamma subfamily C, 5	NM_018929	2.24E-21	0.00182203	1.23154	100
PYGM	Phosphorylase, glycogen; muscle (McArdle syndrome, glycogen	NM_005609	7.14E-19	0.000661684	1.64136	20
SEMA5B	Sema domain, seven thrombospondin Repeats (type 1 and	NM_001031702	6.12E-25	0.746505	1.02067	31
SF1	Splicing factor 1	NM_004630	3.25E-18	0.0117229	1.26463	32
SLC1A3	Solute carrier family 1 (glial high affinity glutamate transporter)	NM_004172	3.81E-05	0.000106293	2.50395	15
SLC35A4	Solute carrier family 35, member A4	NM_080670	0.793629	7.95E-05	-1.49356	8
SLC4A4	Solute carrier family 4, sodium bicarbonate co-transporter	NM_001098484	1.64E-16	0.000145173	2.17261	31
TJP2	Tight junction protein 2 (zona occludens 2)	NM_004817	9.14E-16	0.000452437	2.01894	31
TRBV19	T-cell receptor beta variable 19	BC073930	1.48E-15	0.695085	1.02684	30
UTRN	Utrophin	NM_007124	1.56E-20	0.00473928	1.78074	74

adhesion (enrichment $P = 10^{-31}$ versus $P = 10^{-12}$, respectively). When examining the 57 genes identified by cell adhesion, genes encoding transmembrane ($n = 24$) and secreted ($n = 21$) proteins were more highly represented than genes encoding nuclear ($n = 2$) or cytoplasmic ($n = 10$) proteins (Table 4). Most of these 57 genes ($n = 52$) were up-regulated and only a few ($n = 5$) were down-regulated, although the up- and down-regulation did not always meet statistical significance (Fig. 3 and Table 4). A large number of genes were associated with integrin signaling, representing both ligands (collagens, laminins, fibronectin) and receptors.

There are no clearly identifiable gene signals in the anterior horn enriched mRNA pool

As previously stated, involvement of the microenvironment ('non-neuronal neighbors') is an important aspect of ALS pathobiology in transgenic mice expressing mutant SOD1 (3) and thus to study it in SALS, we collected and profiled the entire anterior horn after removal of motor neurons. We had comparable quality of data as the motor neuron enriched mRNA pool (Supplementary Material S1) but when applying the same bioinformatics analyses that we used for the motor

Table 3. Biological enrichment of aberrantly spliced genes

Enrichment	Enrichment <i>P</i> -value	% genes in group that are present	Number of genes present	Number of genes in group	GO ID	GO category
Biological adhesion	10 ⁻⁵⁸	8.6758	57	657	22610	BP
Cell adhesion	10 ⁻⁵⁸	8.6758	57	657	7155	BP
Basement membrane	10 ⁻⁴⁸	28.9474	11	38	5604	CC
Transmembrane receptor protein tyrosine kinase activity	10 ⁻⁴³	20.5882	14	68	4714	MF
Collagen	10 ⁻⁴³	28.5714	10	35	5581	CC
Extracellular matrix structural constituent	10 ⁻⁴²	18.75	15	80	5201	MF
Vascular endothelial growth factor receptor activity	10 ⁻⁴²	50	6	12	5021	MF
Laminin-1 complex	10 ⁻⁴¹	62.5	5	8	5606	CC
Laminin complex	10 ⁻⁴¹	62.5	5	8	43256	CC
Transmembrane receptor protein kinase activity	10 ⁻⁴¹	18.2927	15	82	19199	MF
Regulation of cell migration	10 ⁻³⁹	29.0323	9	31	30334	BP
Cell-substrate adhesion	10 ⁻³¹	17.3913	12	69	31589	BP
Cell-matrix adhesion	10 ⁻²⁸	17.1875	11	64	7160	BP
Extracellular region part	10 ⁻²⁷	6.38003	46	721	44421	CC
Protein binding	10 ⁻²⁷	3.32847	228	6850	5515	MF
Plasma membrane part	10 ⁻²⁵	4.74517	81	1707	44459	CC
Regulation of cell motility	10 ⁻²⁵	14.2857	12	84	51270	BP
Cell-substrate junction assembly	10 ⁻²⁵	60	3	5	7044	BP
Cell junction assembly	10 ⁻²⁵	60	3	5	34329	BP
Extracellular matrix organization and biogenesis	10 ⁻²⁴	19.5122	8	41	30198	BP
Collagen binding	10 ⁻²³	29.4118	5	17	5518	MF
Phosphate transport	10 ⁻²³	13.1868	12	91	6817	BP
Hemidesmosome	10 ⁻²³	100	2	2	30056	CC
Integrin-mediated signaling pathway	10 ⁻²³	16.3636	9	55	7229	BP
Proteinaceous extracellular matrix	10 ⁻²²	9.00901	20	222	5578	CC
Regulation of embryonic development	10 ⁻²²	50	3	6	45995	BP
Stereocilium	10 ⁻²²	50	3	6	32420	CC
Fibroblast growth factor receptor activity	10 ⁻²²	50	3	6	5007	MF
Extracellular matrix	10 ⁻²¹	8.77193	20	228	31012	CC
Anatomical structure development	10 ⁻²¹	5.15464	55	1067	48856	BP
Structural molecule activity	10 ⁻²¹	5.91716	40	676	5198	MF
Integrin complex	10 ⁻²⁰	21.4286	6	28	8305	CC
Developmental process	10 ⁻²⁰	4.04485	101	2497	32502	BP

BP, biological process; MF, molecular function; CC, cellular component.

neuron enriched pool, we could not identify any mRNA gene signals above noise levels either by way of differential gene expression, aberrant splicing, or biological enrichment (Supplementary Material S3), thus demonstrating the compartment-specific nature of our findings. To better understand this lack of signal in the anterior horn, we examined our analogous G93A mouse data that used 3' gene expression arrays and determined signal strength in the anterior horn and in motor neuron enriched mRNA pools isolated by microdissection using a similar bioinformatics analysis. At both 20 and 60 post-natal days, we identified significant and comparable numbers of differentially expressed genes above experiment-specific noise levels in both pools (data not shown), thus demonstrating different strengths of genomic expression in the relevant histological compartments between mouse SOD1 and human SALS samples.

The biological enrichments of aberrant exon splicing in SALS and in an SMA mouse model of motor neuron degeneration are highly concordant

Recently, exon splicing in a mouse model of SMA motor neuron degeneration using whole genome exon arrays demonstrated widespread tissue-specific aberrant splicing, supporting the hypothesis that functional loss of the SMN1 protein in

spliceosomes and aberrant splicing are fundamental in disease pathogenesis (24). To compare our findings to those in this study in uniform manner, we downloaded the CEL files of the spinal cord tissues from this study and processed them the same way we processed our own. With the bioinformatics approach reported in the study, 259 genes were identified as being aberrantly spliced in the spinal cord. Using our bioinformatics approach estimating data-specific noise thresholds, 74 genes were identified (data not shown). By either approach, there was significant aberrant splicing in degenerating tissues. There was a greater degree of aberrant splicing in our human SALS tissues ($n = 411$) than in the SMA mouse model tissues ($n = 74$), a difference likely due to greater compartment specificity in our study using microdissection. While this supports emerging ideas about a role of exon splicing in motor neuron diseases, in fact the ability to detect global splicing alterations is relatively recent with the development of exon arrays and few studies have been reported. To better understand this, we next compared the SALS and SMA data with others recently reported in the literature in non-motor neuron disease conditions (31,32). We downloaded CEL files from these studies and processed them the same way we processed our own data. We found even greater degrees of aberrant gene splicing occurring in these other conditions (data not shown), thus reinforcing that important biologic functions relate to exon splicing.

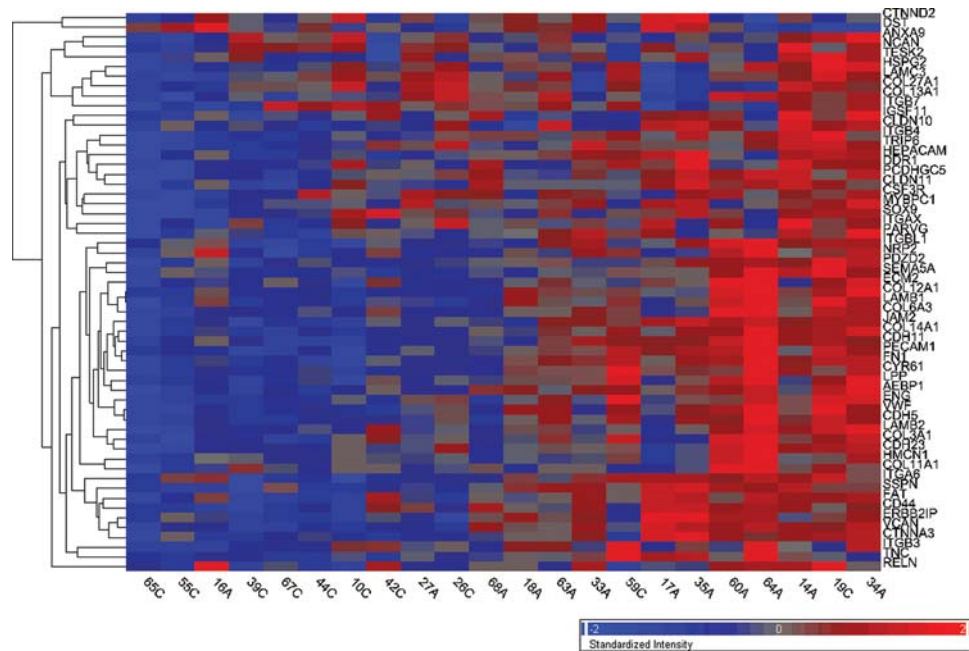


Figure 3. Heat map of the gene expression levels of the 57 cell adhesion genes identified by their aberrant splicing in the motor neuron enriched mRNA pool in our study. These 57 genes comprise the cell adhesion biological pathway as defined in the Gene Ontology. They were identified in our study by virtue of their marked over-representation in the 411 aberrantly spliced genes identified in the motor neuron enriched mRNA pool in SALS ($P < 10^{-57}$). The colored bar indicates the range of intensity values for each gene and the heat maps display their overall gene expression levels, not their aberrant splicing. Note the relatively clean separation of SALS and control groups and the preponderant up-regulation or over-expression of these genes, which is seen in addition to their aberrant splicing. (C, control and A, SALS).

This functional specificity of exon splicing is clearly supported by enrichment analyses. The SMA mouse model study also identified enrichment of ECM biology in the cohort of aberrantly spliced genes, although quantitative analysis was not presented and the finding was not emphasized. To compare our findings to the ones reported in this study in uniform manner, we sought enrichment the same way we sought it in ours and we noted comparably robust enrichment: in the SMA study, we identified 26 gene sets with enrichment $P \leq 10^{-20}$, the cutoff we calculated for their noise. Some gene sets had enrichment P -values $< 10^{-78}$. The specific enrichments were dominantly related to ECM, collagen, cell adhesion, and related functions (Supplementary Material S2). While the 26 gene sets with enrichment $P \leq 10^{-20}$ contained a total number of 185 genes, many genes appeared redundantly in the gene sets and only 48 were unique. Of these, 32 specifically relate to ECM, cell adhesion, and related functions. Of the 48 unique genes from the SMA study and the 111 unique genes from our SALS study identified by the respective enrichment analyses, only 5 overlapped (col12a1, coll14a1, fn1, hspg2 and itgb4) (Supplementary Material S2).

TARDBP/TDP-43, TDP-43 targets and other genes of ALS interest are mostly normal

We interrogated our data for currently known genes of interest in SALS pathobiology. A 1.5-fold change of TARDBP has been previously reported in brains of frontotemporal lobar dementia with ubiquitinated pathology using microarray

analysis, although the replicates were small and tissue was not cell-specific (33). In our array data, we also found that this might be true in the motor neuron enriched mRNA pool (1.3-fold change with $P = 0.008$) but not the anterior horn enriched mRNA pool, but subsequent qPCR of all 12 SALS and 10 controls samples did not validate this (data not shown). TARDBP was normally spliced and we therefore conclude TARDBP mRNA transcription is normal in SALS. We also interrogated our data for known targets of TDP-43—CFTR, APO A-II, and CDK6—and we found they were neither differentially expressed nor aberrantly spliced. The representations for SMN1 and SMN2 are sparse on the array and what little could be assayed did not demonstrate differential gene expression (aberrant splicing could not be determined). We also interrogated our data for currently known genes of interest in FALS and motor neuron disease biology other than TARDBP—SOD1, FUS/TLS, SETX, ATXN7, IGHMBP2, ELP3 and ANG—and they were neither differentially expressed nor aberrantly spliced. As the targets of these genes are largely unknown, we cannot comment further on their possible aberrant splicing. Glycyl-tRNA synthetase (GARS), which is of putative interest in ALS (22), appeared to demonstrate significant down-regulation (-1.4 -fold change with $P = 0.0006$) by microarray but this was not validated by subsequent qPCR (data not shown). In addition, we looked at genes identified by the Gene Ontology as involved in RNA processing and identified 39 genes as being either aberrantly spliced or differentially expressed, although this biological category was not abnormally enriched by enrichment analysis. We also found that the glutamate transporter

Table 4. Aberrantly spliced cell adhesion genes

Gene symbol	Gene name	RefSeq	Alt. splice <i>P</i> -value	Differential expression <i>P</i> -value	Fold change (A versus C)	Number of markers	Protein location
AEBP1	AE binding protein 1	NM_001129	2.44E-10	0.0186655	1.69315	27	sec
ANXA9	Annexin A9	NM_003568	8.62E-07	0.971328	-1.00249	14	cyt
CDH11	Cadherin 11, type 2, OB-cadherin (osteoblast)	NM_001797	2.94E-06	0.00458728	1.65623	21	tm
CDH5	Cadherin 5, type 2, VE-cadherin (vascular epithelium)	NM_001795	2.36E-06	0.102509	1.27449	19	tm
CDH23	Cadherin-like 23	NM_022124	1.61E-07	0.156179	1.12818	71	tm
CTNNA3	Catenin (cadherin-associated protein), alpha 3	NM_013266	6.53E-06	0.00648134	1.79781	25	cyt
CTNND2	Catenin (cadherin-associated protein), delta 2	NM_001332	1.59E-06	0.0867763	1.1616	32	cyt
CD44	CD44 molecule (Indian blood group)	NM_000610	5.13E-12	0.000479249	1.89535	21	tm
CLDN10	Claudin 10	NM_182848	6.03E-06	0.162268	1.20723	12	tm
CLDN11	Claudin 11 (oligodendrocyte transmembrane protein)	NM_005602	1.94E-06	0.00435624	1.53442	6	tm
COL3A1	Collagen, type III, alpha 1 (Ehlers-Danlos syndrome type)	NM_000090	3.84E-09	0.221719	1.17435	49	sec
COL6A3	Collagen, type VI, alpha 3	NM_004369	3.34E-20	0.0945555	1.36456	45	sec
COL11A1	Collagen, type XI, alpha 1	NM_001854	2.33E-09	0.178053	1.20705	46	sec
COL12A1	Collagen, type XII, alpha 1	NM_004370	1.69E-10	0.0105983	1.79078	69	sec
COL13A1	Collagen, type XIII, alpha 1	NM_005203	6.71E-09	0.169929	1.15626	25	sec
COL14A1	Collagen, type XIV, alpha 1 (undulin)	NM_021110	1.06E-08	0.00638787	1.58704	24	sec
COL27A1	Collagen, type XXVII, alpha 1	NM_032888	1.43E-06	0.243964	-1.10262	46	sec
CSF3R	Colony stimulating factor 3 receptor (granulocyte)	NM_156039	2.04E-06	0.126098	1.10957	24	tm
CYR61	Cysteine-rich, angiogenic inducer, 61	NM_001554	1.17E-07	0.0315499	1.55961	8	sec
DDR1	Discoidin domain receptor family, member 1	NM_013993	4.24E-08	0.103136	1.15821	31	tm
DST	Dystonin	NM_183380	9.73E-24	0.323111	1.0925	125	cyt
ENG	Endoglin (Osler-Rendu-Weber syndrome 1)	NM_000118	5.65E-06	0.342529	1.19248	20	tm
ERBB2IP	ErbB2 interacting protein	NM_018695	6.83E-07	0.000240051	2.08535	30	cyt
ECM2	Extracellular matrix protein 2, female organ and adipocyte	NM_001393	4.60E-06	0.0461937	1.59777	20	sec
FAT	FAT // FAT tumor suppressor homolog 1 (Drosophila)	NM_005245	1.45E-08	0.00159728	1.86066	31	tm
FN1	Fibronectin 1	NM_212482	2.24E-21	0.0133788	2.50828	63	sec
HMCN1	Hemicentin 1	NM_031935	7.81E-07	0.209353	1.1854	116	sec
HSPG2	Heparan sulfate proteoglycan 2	NM_005529	2.11E-09	0.938373	-1.00658	101	sec
HEPACAM	Hepatocyte cell adhesion molecule	NM_152722	2.96E-06	0.0223096	1.54885	13	tm
IGSF11	Immunoglobulin superfamily, member 11	NM_001015887	5.57E-08	0.0724414	1.24835	13	tm
ITGA6	Integrin, alpha 6	NM_000210	9.56E-08	0.0229754	2.06743	29	tm
ITGAX	Integrin, alpha X (complement component 3 receptor 4 subunit)	NM_000887	7.10E-08	0.305373	1.09177	29	tm
ITGB3	Integrin, beta 3 (platelet glycoprotein IIIa, antigen CD61)	NM_000212	1.12E-06	0.394661	1.16482	20	tm
ITGB4	Integrin, beta 4	NM_000213	4.07E-15	0.183707	1.14822	44	tm
ITGB7	Integrin, beta 7	NM_000889	1.28E-12	0.345837	-1.07065	17	tm
ITGBL1	ITGBL1 // integrin, beta-like 1 (with EGF-like repeat domains)	NM_004791	2.24E-14	0.00392462	1.97861	16	tm
JAM2	Junctional adhesion molecule 2	NM_021219	3.87E-08	0.00548407	2.02731	13	tm
LAMB1	Laminin, beta 1	NM_002291	2.61E-13	0.0290629	1.61794	36	sec
LAMB2	Laminin, beta 2 (laminin S)	NM_002292	3.16E-06	0.155571	1.21405	40	sec
LAMC3	Laminin, gamma 3	NM_006059	8.59E-06	0.370666	-1.06083	35	sec
LPP	LIM domain containing preferred translocation partner in lip	NM_005578	1.40E-06	0.147014	1.51955	13	cyt
MYBPC1	Myosin binding protein C, slow type	NM_002465	1.90E-21	0.00967833	1.31138	31	cyt
NCAN	Neurocan	NM_004386	4.77E-10	0.206516	1.13639	25	sec
NRP2	Neuropilin 2	NM_003872	5.65E-07	0.0447044	1.29315	36	tm
PARVG	Parvin, gamma	NM_022141	2.03E-07	0.015984	1.25824	14	cyt
PDZD2	PDZ domain containing 2	NM_178140	2.86E-07	0.0529539	1.34362	44	cyt
PECAM1	Platelet/endothelial cell adhesion molecule (CD31 antigen)	NM_000442	3.50E-06	0.023662	2.42764	17	tm
PCDHGC5	Protocadherin gamma subfamily C, 5	NM_018929	2.24E-21	0.00182203	1.23154	100	tm
RELN	Reelin	NM_173054	3.03E-06	0.0459772	1.59369	73	sec

Continued

Table 4. Continued

Gene symbol	Gene name	RefSeq	Alt. splice P-value	Differential expression P-value	Fold change (A versus C)	Number of markers	Protein location
SSPN	Sarcospan (Kras oncogene-associated gene)	NM_005086	1.23E-07	0.00153469	1.87677	8	tm
SEMA5A	Sema domain, seven thrombospondin Repeats	NM_003966	6.24E-06	0.132723	1.27857	29	tm
SOX9	SRY (sex determining region Y)-box 9 (campomelic dysplasia)	NM_000346	3.07E-07	0.584737	1.05446	9	nuc
TNC	Tenascin C (hexabrachion)	NM_002160	2.55E-08	0.125224	1.66206	36	sec
TESK2	Testis-specific kinase 2	NM_007170	6.75E-07	0.0632463	1.36536	14	nuc
TRIP6	Thyroid hormone receptor interactor 6	NM_003302	2.74E-07	0.194651	1.16145	13	cyt
VCAN	Versican	NM_004385	8.36E-11	0.000148832	2.61415	26	sec
VWF	von Willebrand factor	NM_000552	5.40E-12	0.085195	1.51082	46	sec

cyt, cytoplasmic; nuc, nuclear; sec, secreted; tm, transmembrane.

EAAT2 (SLC1A2), which is potentially aberrantly spliced in ALS (34) was not abnormal, consistent with another report (35); however, we did observe that two other glutamate transporters, EAAT1 (SLC1A3) and EAAT4 (SLC1A6) might be differentially expressed (2.5-fold change with $P = 0.0001$ and -1.2 -fold change with $P = 0.007$, respectively) and both validated by qPCR ($P = 0.025$) (Supplementary Material, S2).

qPCR validates microarray predictions of aberrantly spliced gene candidates

In order to validate aberrant exon splicing between the SALS and control as predicted by the exon arrays, 12 candidate genes were selected and exons within these genes predicted to exhibit differences and lack of difference were both assayed by TaqMan qPCR (see Materials and Methods). These genes were chosen from a variety of biological pathways to assay for splicing differences in various biological processes (Supplementary Material S4). Eight out of the 12 genes or 67% (EDNRB, PAX6, SF1, TMBIM1, TRBV19, VCAN, ARHGAP15 and AQP4) as illustrated in Figure 4 showed both of the changes predicted by the exon array in the same gene (Supplementary Material S4). This level of PCR validation is consistent with or above those in similar exon array studies (36–38) and we are thus reassured of the validity of the exon array predictions.

DISCUSSION

We made three key observations, the foundation of which is summarized in Table 5. The first key observation is that genomic abnormalities in SALS are highly localized to the motor neuron enriched mRNA pool (the degenerating anatomic compartment) and not apparent in the anterior horn enriched mRNA pool (the surrounding microenvironment). The strength of signal in the former and the lack of signal in the latter (which is itself enriched by removal of nearly 75% of the surrounding spinal cord) show this and the critical importance of anatomic and technical precision in identifying pathologic changes *in vivo*. The exact identity of the motor

neuron enriched mRNA pool is not entirely clear. In favor of its mRNA deriving mostly from motor neurons is the anatomic specificity of microdissection and our preliminary histological studies of these same tissues in FFPE that do not show obvious surrounding hypercellularity. In favor of its containing mRNA also from non-motor cells is the difficulty of resolving cell morphology in the frozen cryosections on which microdissection is performed, the identification of biological enrichment that may be external to the cell itself (cell–adhesion, cell–matrix and ECM), and the identification of a number of genes that appear to be primarily glial. Thus, while enriched in microdissected motor neurons, it is possible that the mRNA signals are also enriched in other proximate cells or their mRNA-rich processes.

A striking finding is lack of signal and biologic enrichment in the anterior horn enriched mRNA pool. While this lack of signal validates our strategic approach of separating the two compartments, it is surprising given the strong evidence indicating that motor neuron degeneration is non-autonomous in mice expressing mutant SOD1 (3,4) and the strong evidence supporting the role of glia in magnifying the motor neuron pathology associated with ALS (39–41). In our comparable data from mutant SOD1 transgenic mice, we did in fact show equal signal strengths between the motor neuron and the anterior horn enriched mRNA pools. There are a number of potential explanations for this difference in human disease and the mutant SOD1 transgenic mouse model. In humans, the anterior horn is much larger anatomically than in mice and the critical interactions may reside in very close apposition to the neurons and thus detectable in the motor neuron enriched mRNA pool but diluted in the anterior horn enriched mRNA pool. In humans, the larger-sized anterior horn compared with mice may allow greater cellular heterogeneity and greater noise. In humans, the changes are sequential and summing, whereas in mice they are temporally synchronized. In humans, the effects in the anterior horn may be subtler than in mice and not detectable with our bioinformatics-based approach. Or, of course, non-autonomous cell effects may not be as significant in SALS pathogenesis as in the SOD1 mouse model, upon which most of the non-autonomous cell degeneration literature is based.

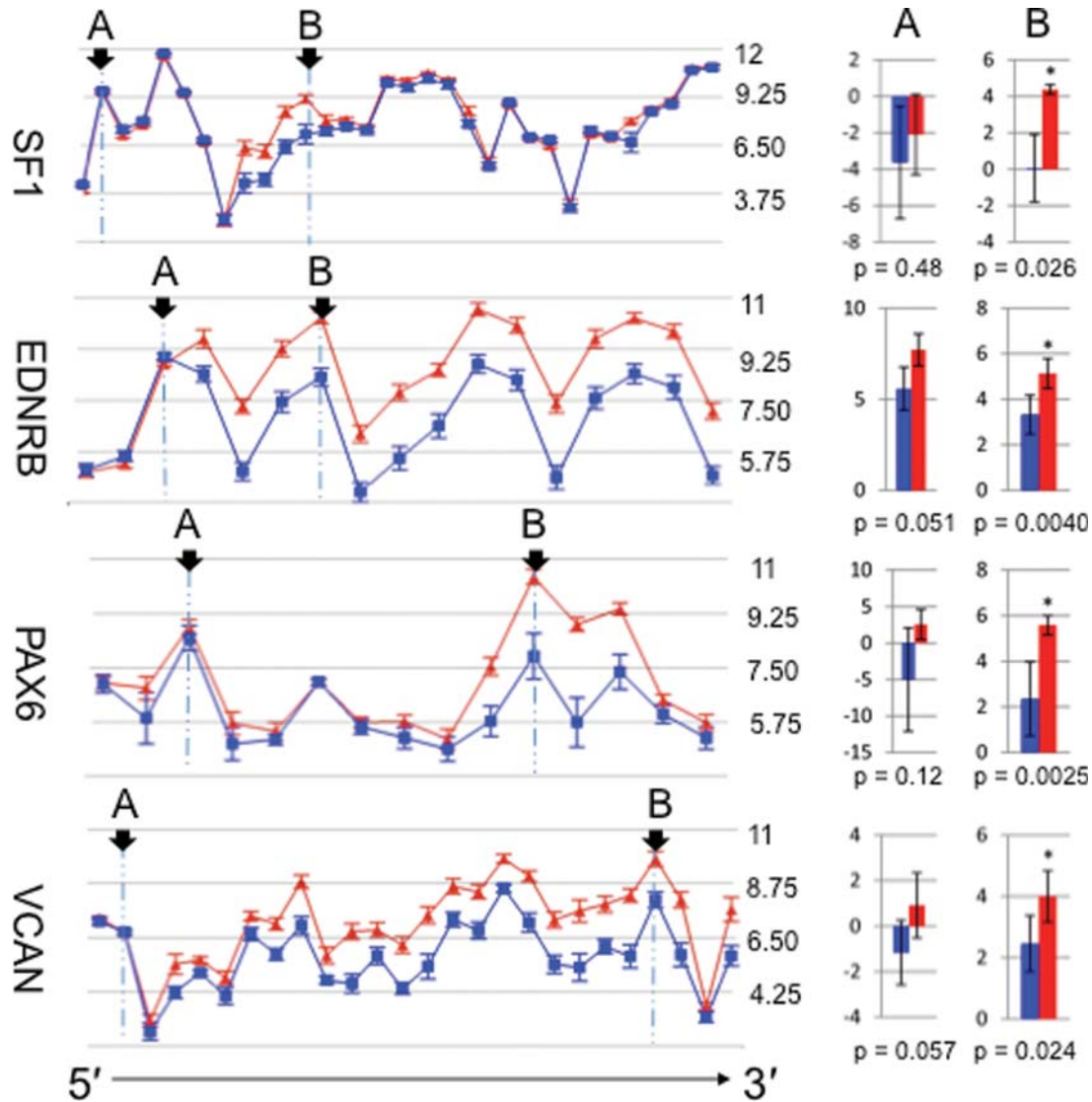


Figure 4. Aberrant splicing predictions of the exon arrays validate by qPCR. Four examples of validation of aberrant splicing are demonstrated in this figure. The gene views on the left show the expression of exons as determined by exon array; the expression levels are shown on a \log_2 scale; the error bars show standard errors of means; SALS, red triangles; control, blue squares. Exons showing similar (A) and different (B) expression between SALS and control (arrows) were selected for validation by qPCR. The bar plots on the right show the results of qPCR: expression of the selected exons are normalized to GAPDH and shown on a \log_2 scale; the error bars show the 95% confidence intervals; SALS, red; control, blue. Asterisks indicate significant difference by *t*-test ($\alpha = 0.05$) in expression as predicted by the microarray. In these examples, exons predicted to have differential expression and exons predicted not to have differential expression were confirmed by qPCR.

The second key observation of our study is that exon splicing is more significant and relevant than differential gene expression in SALS—signals are more clearly identified and their biological enrichment more robustly defined by profiling aberrant exon splicing than differential gene expression. This supports the critical biological (6–8) and pathologic (10) importance of exon splicing in general and its interest to ALS (14–24) in particular. TDP-43 is the leading candidate in SALS pathogenesis and its exact role in pathogenesis is fundamental but remains unclear (14). Since one of its main known functions is exon splicing and in SALS it mislocalizes from the nucleus to the cytoplasm, it is important to note that we could not detect expression or splicing changes in its

encoding gene TARDBP or any of its known targets including CFTR, APO A-II, CDK6 and SMN1. Together, these suggest that its role in SALS pathobiology is not likely at its own mRNA level and that it likely involves some other yet-to-be-identified targets or mechanisms—to date, a comprehensive list of TDP-43 targets and actions has not been defined. Alternatively, TDP-43 may involve functions other than exon splicing and the importance of the aberrant splicing that was detected by us is separate. The important role exon splicing may play in motor neuron degeneration is highlighted by SMA (42). SMA is caused by homozygous loss of the SMN gene, which is essential for biogenesis of small nuclear ribonucleoprotein particles that are critical components of the RNA

Table 5. Summary of key findings

	Motor neuron enriched mRNA pool	Anterior horn enriched mRNA pool
Cellularity	Homogeneous (single-cell enriched)	Heterogeneous (glia, endothelium, small neurons, degenerating neurons)
Anatomic size	Highly discrete	Comparatively vast
Differential gene expression	148 genes	Not detectable above noise
Biological enrichment of differentially expressed genes	Not detectable above noise	Not detectable above noise
Aberrant exon splicing	411 genes	Not detectable above noise
Biological enrichment of aberrantly spliced genes	Cell–matrix adhesion and extracellular matrix biology; also transmembrane receptor protein tyrosine kinase activity, vascular endothelial growth factor receptor activity, and regulation of cell motility	Not detectable above noise

splicing apparatus (43). Thus, splicing abnormalities are expected to play major roles in motor neuron degeneration and have been demonstrated in a mouse model to be both widespread and tissue-specific, differing within different neuronal tissues and between neuronal and non-neuronal tissues (24). Together with our study, splicing abnormalities are shown to be cell-specific as well as tissue-specific.

The mechanistic bases of the aberrant splicing in ALS are unclear. A number of RNA processing factors are themselves aberrantly spliced or differentially expressed in our SALS samples (Supplementary Material S2), which may provide an explanation for at least part of the splicing changes in SALS. We do not know if the genes encoding these RNA processing factors are mutated in SALS, similar to FUS/TLS or TDP-43, or if they are abnormally regulated downstream of primary disease-causing genes, but they represent interesting candidates for further analysis. For example, SF1 and SFRS2 have been shown to associate with FUS/TLS (44,45) and SFRS2 also alters the splicing of the TDP-43 target APO A-II (46), while SFRS5 alters the splicing of two TDP-43 targets (APO A-II and CFTR) (46,47). In addition, ELAVL3 (HuC) has a role in paraneoplastic neurologic disorders (48) and neuronal development (49). Interestingly, mutant SOD1 competes with HuC (and HuR) for binding to the 3'-UTR of vascular endothelial growth factor (VEGF) (50). RNASET2 is of interest due to the potential role of angiogenin (also an RNase) in ALS (22), as well as the recently demonstrated effects of RNASET2 loss on neuronal development (51). PTPBP1 represents a key regulator of neuronal development through its effects on repressing neural PTP (also called PTBP2) (52), as loss of PTPBP1 results in neural differentiation associated with PTPBP2 activation (53). There

is also recent evidence of PTPBP1 involvement in the proliferation and migration of gliomas (54).

The third key observation of our study is the specific identification in SALS of perturbation of cell adhesion and ECM biology, especially cell–matrix as opposed to cell–cell adhesion genes. Other identified pathways included transmembrane receptor protein tyrosine kinase activity, vascular endothelial growth factor receptor activity [already of great interest in ALS pathobiology (55)] and regulation of cell motility (Tables 3 and 5). Since these were only identified in the motor neuron enriched mRNA pool and not in the larger surroundings of the anterior horn, their gene action is at or very proximate to neurons. Most of the cell adhesion genes we identified encode proteins that are either secreted or transmembrane as opposed to cytosolic or nuclear. The mechanisms by which these genes are likely to exert their effects are on the structure of the encoded proteins because the key to their identification was the aberrant splicing of the exons in the genes encoding them. Their abnormal action is likely to be part of an active rather than passive process since they are also mostly over-expressed or up-regulated. Where in the cascade of motor neuron degeneration their perturbations occurs or whether their perturbations are primary or secondary are unknown—their identification depended on pooling motor neurons within each nervous system and analysis of signals among multiple nervous systems. But the perturbations arguably are relatively upstream: (i) studies were performed in regions to which the degenerative process was newly advancing and therefore neuron-rich (in fact, these studies are only feasible in such regions) (26); (ii) the neurons in these regions showed relatively inconspicuous changes histologically when examined in companion FFPE tissues; and (iii) microdissection has an intrinsic bias for selectively collecting larger and healthier motor neurons. The studies on the mouse model of SMA highlight the functional and biological importance of the specific perturbations of cell–matrix and ECM biology: what is most concordant between SALS and SMA motor neuron degeneration is not aberrant exon splicing *per se*—there are only five genes that overlap—but the nearly identical and highly robust biological enrichments of the two distinct aberrant spliced gene cohorts. The source and coordination of the aberrant splicing is unknown and would only be identified by our method if altered in either expression or splicing. While we did observe alterations of RNA processing factors (mentioned above and Supplementary Material S2), there are many other possible alterations such as point mutations or post-translational changes that we are not able to observe. It is even possible, as demonstrated by SMA, that alterations in only one factor could cause multiple splicing abnormalities, but for the same reasons we might not be able to detect such.

Motor neurons are surrounded by a rich structural as well as cellular matrix and there are a number of potential scenarios where altered cell–matrix interactions could significantly affect neuron function. Disruption of cell–matrix molecules could adversely affect glia as well as neurons, thus resulting in or resulting from dysfunction of both cell categories (56). A few possibilities are outlined. (i) Alterations in the ECM could aberrantly modify the diffusion kinetics of paracrine factors such as growth factors, purines, etc., resulting in too

much or too few of these factors reaching adjacent cells (57). (ii) Alterations in ECM could adversely affect neurons via integrin adhesion and signaling (58). (iii) Cell–matrix interactions are critical for neuronal migration, which occurs primarily during development as neural progenitor cells migrate to their proper positions before differentiating (59). Abnormal cell–matrix interactions could alter the normal formation and wiring of the nervous system, thus priming a delayed failure (60). (iv) Alterations in the ECM might cause or reflect derangements to the release of or diffusion of chemoattractants that activate neural progenitor cells and promote their migration toward diseased structures to try to ‘rescue’ degenerating motor neurons (61); alterations in the ECM might allow propagation of a maladapted process. (v) The basal lamina in the CNS, which is comprised predominantly of ECM proteins, serves an important role in modulating the permeability of the blood brain barrier (62). Cleavage of proteins in the basal lamina by matrix metalloproteinases produced by invading inflammatory cells is required to facilitate their access to the CNS (63), thus alterations in ECM protein isoforms could alter blood brain barrier permeability. In addition, we have found that a protein crucial for determining the water permeability of the blood brain barrier, aquaporin-4 (62), demonstrates increased expression of a specific isoform in SALS (see Results). Overexpression of aquaporin-4 has been reported in ALS mouse (64) and rat models (65). It is interesting to note evidence from mouse ALS models indicating blood brain barrier changes early in the disease process (66). And (vi), ECM proteins can directly affect cells or alter the interactions of other ECM proteins with adjacent cells. For example, the ECM protein versican, which demonstrates altered splicing in SALS (see Results), is thought to restrict neuronal plasticity in adults as a component of perineuronal nets (67,68) and is upregulated in a rat model of ALS (66). Additionally, versican promotes the assembly of hyaluronan (69), which can activate microglia through binding to the CD44 receptor (70) (which also undergoes altered splicing in SALS).

These three key observations of our study are especially interesting in light of our recent postulations that motor neuron degeneration in SALS is an actively spreading and propagating process (71). That the aberrantly spliced genes are up-regulated is consistent with the process being active rather than passive. That the aberrantly spliced genes have perturbed cell–matrix and ECM adhesion biology is consistent with the importance of interactions in the microenvironment that could advance in space and over time. In this regard, it is important to note that there are two general types of inter-neuronal communication: one is synaptic communication between neurons that are in series (such as between upper and lower motor neurons or between neurons and interneurons) and the other is local side-to-side communication between neurons that are in parallel and involves local paracrine signaling and the neuron microenvironment. The recent identification that one or more soluble factors are selectively toxic to motor neurons is especially intriguing (72). One of many scenarios that can be imagined is that perturbed cell adhesion induces local changes and release of toxic soluble factors recruiting nearby cells, thus propagating a non-accelerating pathologic process. In the final analysis, our find-

ings do not distinguish primary from secondary changes in pathobiology and add more pieces to the complex puzzle. Many challenges and questions remain, an immediate one being biological validation of our largely bioinformatics-based findings.

MATERIALS AND METHODS

Tissue acquisition and repository

All nervous systems were acquired by way of an Investigational Review Board and Health Insurance Portability and Accountability Act compliant process. The SALS nervous systems were from patients who had been followed during the clinical course of their illness and met El Escorial criteria for definite ALS (73). Upon death, autopsies were performed immediately by an on-call tissue acquisition team. Control nervous systems were from patients from the hospital’s critical care unit when life support was withdrawn (7), patient on hospice (1) and from the Pennsylvania Tissue Repository (2). Tissue collections were completed within 6 h, usually within 4 h, of death and the entire motor system was dissected and elaborately archived for downstream applications by creating two parallel tissue sets from alternating adjacent regions. For molecular studies, segments were embedded in cutting media, frozen on blocks of dry ice and stored at -80°C . For structural studies, the adjacent segments were fixed in 70% neutral buffered formalin, embedded in paraffin (formalin-fixed paraffin-embedded or FFPE) and stored at room temperature.

Microdissection and total RNA isolation

Thirty to forty 8–10 μm cryocut frozen tissue sections stained with cresyl violet acetate were microdissected from each nervous system on a Pixcell Iie Laser Capture Microdissection (LCM) System (Arcturus Bioscience) in a 2-h long epoch for the motor neuron enriched RNA pool. Microdissected cells were captured on CapSureTM Macro LCM Caps (Arcturus Bioscience). After completion of LCM, the surrounding remaining anterior horn region was collected to create a second parallel RNA pool. RNA isolations were based on a guanadinium isothiocyanate and 2-mercaptoethanol extraction and column purification with RNeasy[®] Micro Kit (Qiagen).

mRNA amplification and exon array hybridization

For exon profiling, total RNA was amplified to cDNA probe using random priming with WT-OvationTM Pico RNA Amplification System (NuGEN). The antisense–sense orientation was converted to sense transcript-cDNA (ST-cDNA) using WT-OvationTM Exon Module (NuGEN). ST-cDNA was fragmented and biotin labeled using FL-OvationTM cDNA Biotin Module v2 (NuGEN). Probe was hybridized to GeneChip[®] Human Exon 1.0 ST Arrays (Affymetrix). This array determines both exon and gene expression and are more resilient to RNA degradation changes than traditional 3’ gene arrays, which depend solely on integrity of the 3’ exon (74). Hybridized chips were stained and washed on a GeneChip

450 fluidics Station (Affymetrix) and scanned with a GeneChip 3000 scanner (Affymetrix). Initial data was processed to CEL files using GCOS Version 1.4 (Affymetrix). The microarray data presented herein and deposited in the GEO is MIAME compliant.

Quality control

RNA quality were assessed using digital microelectrophoresis with either a PicoChip™ or NanoChip™ (Agilent), which generated electropherograms, digital gels, and RNA Integrity numbers (RINs) (75). RNA quality was ascertained at each stage of processing—acquisition, microdissection, amplification, fragmentation—and studies were advanced only if optimal. Microarray quality was assessed by visualization of the microarray CEL files, percent positive calls on the microarray, area under the curve (AUC) values, distribution histograms of non-normalized expression scores, box plots of mean and 25th and 75th percentiles probe scores before and after quantile normalization, median normalized non-background corrected scores of probes designated as background, graphs of mean absolute difference between transformed background-corrected and normalized probe scores and frequency histograms of GC counts (76).

Bioinformatics

Primary bioinformatics analysis used Genomics Suite Version 6.4 (Partek). CEL files were imported into the software and their backgrounds underwent RMA and quantile normalizations. Statistical analysis was performed by creating from the individual CEL files two groups, control or SALS, and then comparing them to each other. The exon arrays have three types of probe sets: core, extended and full. The *core probe set* contains ~17 800 transcript clusters and ~284 000 probe sets to RefSeq and GenBank full-length mRNA's; the *extended probe set* contains ~129 000 transcript clusters and ~523 000 probe sets (plus core probes), with additional probes to expressed sequence tags (EST's) and partially annotated mRNA's; and the *full probe set* contains ~262 000 transcript clusters and ~580 000 probe sets (plus core and extended probes) with additional probes to all predicted exons in the genome. For our analysis, we have used the core probe set because of the depth of annotation available. The software uses a proprietary Exon Splice ANOVA algorithm to calculate both each gene's differential expression, which is determined by a composite expression of all its exons comparing between disease and control, and each gene's exon splice index, which is determined by exon-to-exon comparison between disease and control after correcting for other variables, including overall differential gene expression. Among the factors measured by the ANOVA are batch effects. Signal strengths and noise levels were measured in two ways. First, noise levels specific to our data were estimated by randomly permuting CEL file classifications to create comparisons between sham groups; 10 permutations were performed. Second, multiple test correction was performed by Bonferroni method; these data are reported in the Supplementary Material. Enrichment analysis was determined by generating an enrichment score equal to

the P -value of a χ^2 test comparing identified genes and their biological functionality as defined by Gene Ontology (www.geneontology.org). Heat maps were generated by first summarizing the exons of each gene using the 'gene summary' command, followed by the 'cluster based on significant genes' command. Additional bioinformatics analysis was performed using Expression Console™ Version 1.1 (Affymetrix) and XRAY Version 3.92 (Biotique Systems).

Validation of array results by qPCR

Genes identified as being aberrantly spliced were selected for validation by qPCR. Exons exhibiting significant differences as well as lack of differences of expression between SALS and control were analyzed. Target sequences to these exons were obtained from Affymetrix. To these, primers and probes were designed using Applied Biosystem's Primer Express software program (Applied Biosystems Inc.). In the case of TDP-43, GARS, EAAT1 (SLC1A3), EAAT4 (SLC1A6) and GAPDH, standard TaqMan® probes were used (Applied Biosystems, Inc). qPCR was performed using either a 7900HT Fast Real Time PCR System or a 7500 Real Time PCR system using either a 384 or 96-well format (Applied Biosystems, Inc). Four-fold standard dilution curves were generated on each plate for each probe in an RT step using RNeasy-purified HEK 293 RNA (Qiagen). Test samples consisted of amplified cDNA from the motor neuron enriched RNA pools and were run in triplicate. The resulting data were normalized to endogenous GAPDH run in parallel on each plate. Values from 3–12 SALS and 3–10 control were separately determined, averaged between groups, and compared by two-tailed Welch's t -test using logarithmic scaling. We called a gene valid only if two conditions were both met: an exon predicted to have differential expression and an exon predicted not to have differential expression were confirmed by qPCR.

SUPPLEMENTARY MATERIAL

Supplementary Material is available at *HMG* online.

Conflict of Interest statement. None declared.

FUNDING

This work was supported by grants from Microsoft Research, the National Institutes of Health (NS051738), the Department of Defense (USAMRAA W81XWH-07-0246), the Wyckoff family, the Moyer Foundation, Mrs Lois Caprile and the Benaroya Foundation.

REFERENCES

- Rowland, L.P. and Shneider, N.A. (2001) Amyotrophic lateral sclerosis. *N. Engl. J. Med.*, **344**, 1688–1700.
- Bruijn, L.I., Miller, T.M. and Cleveland, D.W. (2004) Unraveling the mechanisms involved in motor neuron degeneration in ALS. *Annu. Rev. Neurosci.*, **27**, 723–749.
- Boillee, S., Vande Velde, C. and Cleveland, D.W. (2006) ALS: a disease of motor neurons and their nonneuronal neighbors. *Neuron*, **52**, 39–59.

4. Neusch, C., Bähr, M. and Schneider-Gold, C. (2007) Glia cells in amyotrophic lateral sclerosis: new clues to understanding an old disease? *Muscle Nerve*, **35**, 712–724.
5. Liscic, R.M., Grinberg, L.T., Zidar, J., Gitcho, M.A. and Cairns, N.J. (2008) ALS and FTL: two faces of TDP-43 proteinopathy. *Eur J. Neurol*, **15**, 772–780.
6. Blencowe, B.J. (2006) Alternative splicing: new insights from global analyses. *Cell*, **126**, 37–47.
7. Kim, E., Goren, A. and Ast, G. (2008) Alternative splicing: current perspectives. *Bioessays*, **30**, 38–47.
8. Kwan, T., Benovoy, D., Dias, C., Gurd, S., Provencher, C., Beaulieu, P., Hudson, T.J., Sladek, R. and Majewski, J. (2008) Genome-wide analysis of transcript isoform variation in humans. *Nat. Genet.*, **40**, 225–231.
9. Wahl, M.C., Will, C.L. and Lührmann, R. (2009) The spliceosome: design principles of a dynamic RNP machine. *Cell*, **136**, 701–718.
10. Wang, G.S. and Cooper, T.A. (2007) Splicing in disease: disruption of the splicing code and the decoding machinery. *Nat. Rev. Genet.*, **8**, 749–761.
11. Clark, T.A., Schweitzer, A.C., Chen, T.X., Staples, M.K., Lu, G., Wang, H., Williams, A. and Blume, J.E. (2007) Discovery of tissue-specific exons using comprehensive human exon microarrays. *Genome Biol.*, **8**, R64.
12. Shendure, J. (2008) The beginning of the end for microarrays? *Nature Methods*, **5**, 585–587.
13. Lagier-Tourenne, C. and Cleveland, D.W. (2009) Rethinking ALS: the FUS about TDP-43. *Cell*, **136**, 1001–1004.
14. Neumann, M., Sampathu, D.M., Kwong, L.K., Truax, A.C., Micsenyi, M.C., Chou, T.T., Bruce, J., Schuck, T., Grossman, M., Clark, C.M. *et al.* (2006) Ubiquitinated TDP-43 in frontotemporal lobar degeneration and amyotrophic lateral sclerosis. *Science*, **314**, 130–133.
15. Arai, T., Hasegawa, L.M., Akiyama, H., Ikeda, K., Nonaka, T., Mori, H., Mann, D., Tsuchiya, K., Yoshida, M., Hashizume, Y. *et al.* (2006) TDP-43 is a component of ubiquitin-positive tau-negative inclusions in frontotemporal lobar degeneration and amyotrophic lateral sclerosis. *Biochem. Biophys. Res. Commun.*, **351**, 602–611.
16. Buratti, E. and Baralle, F.E. (2008) Multiple roles of TDP-43 in gene expression, splicing regulation, and human disease. *Front. Biosci.*, **13**, 867–878.
17. Sreedharan, J., Blair, I.P., Tripathi, V.B., Hu, X., Vance, C., Rogelj, B., Ackerley, S., Durnall, J.C., Williams, K.L., Buratti, E. *et al.* (2008) TDP-43 mutations in familial and sporadic amyotrophic lateral sclerosis. *Science*, **319**, 1668–1672.
18. Kabashi, E., Valdmanis, P.N., Dion, P., Spiegelman, D., McConkey, B.J., Vande Velde, C., Bouchard, J.P., Lacomblez, L., Pochigaeva, K. *et al.* (2008) TARDBP mutations in individuals with sporadic and familial amyotrophic lateral sclerosis. *Nat. Genet.*, **40**, 572–574.
19. Van Deerlin, V.M., Leverenz, J.B., Bekris, L.M., Bird, T.D., Yuan, W., Elman, L.B., Clay, D., Wood, E.M., Chen-Plotkin, A.S., Martinez-Lage, M. *et al.* (2008) TARDBP mutations in amyotrophic lateral sclerosis with TDP-43 neuropathology: a genetic and histopathological analysis. *Lancet Neurol.*, **7**, 409–416.
20. Kwiatkowski, T.J., Bosco, D.A., LeClerc, A.L., Tamrazian, E., Vanderburg, C.R., Russ, C., Davis, A., Gilchrist, J., Kasarskis, E.J., Munsat, T. *et al.* (2009) Mutations in the FUS/TLS gene on chromosome 16 cause familial amyotrophic lateral sclerosis. *Science*, **323**, 1205–1208.
21. Vance, C., Rogelj, B., Hortobágyi, T., De Vos, K.J., Nishimura, A., Sreedharan, J., Hu, X., Smith, B., Ruddy, D., Wright, P. *et al.* (2009) Mutations in FUS, an RNA processing protein, cause familial amyotrophic lateral sclerosis type 6. *Science*, **323**, 1208–1211.
22. Belezza-Meireles, A. and Al-Chalabi, A. (2008) Genetic studies of amyotrophic lateral sclerosis: controversies and perspectives. *Amyotroph. Lateral Scler.*, **26**, 1–14.
23. Simpson, C.L., Lemmens, R., Miskiewicz, K., Broom, W.J., Hansen, V.K., van Vught, P.W., Landers, J.E., Sapp, P., Van Den Bosch, L., Knight, J. *et al.* (2009) Variants of the elongator protein 3 (ELP3) gene are associated with motor neuron degeneration. *Hum. Mol. Genet.*, **18**, 472–481.
24. Zhang, Z., Lotti, F., Dittmar, K., Younis, I., Wan, L., Kasim, M. and Dreyfuss, G. (2008) SMN deficiency causes tissue-specific perturbations in the repertoire of snRNAs and widespread defects in splicing. *Cell*, **133**, 585–600.
25. Ravits, J., Paul, P. and Jorg, C. (2007) Focality of upper and lower motor neuron degeneration at the clinical onset of ALS. *Neurology*, **68**, 1571–1575.
26. Ravits, J., Laurie, P., Fan, Y. and Moore, D.H. (2007) Implications of ALS focality: rostral-caudal distribution of lower motor neuron loss postmortem. *Neurology*, **68**, 1576–1582.
27. Mirmics, K. and Pevsner, J. (2004) Progress in the use of microarray technology to study the neurobiology of disease. *Nat. Neurosci.*, **7**, 434–439.
28. Jiang, Y.M., Yamamoto, M., Kobayashi, Y., Yoshihara, T., Liang, Y., Terao, S., Takeuchi, H., Ishigaki, S., Katsuno, M., Adachi, H. *et al.* (2005) Gene expression profile of spinal motor neurons in sporadic amyotrophic lateral sclerosis. *Ann. Neurol.*, **57**, 236–251.
29. Curtis, R., Oresic, M. and Vidal-Puig, A. (2005) Pathways to the analysis of microarray data. *Trends in Biotechnology*, **23**, 429–435.
30. Bussemaker, H., Ward, L. and Boorsma, A. (2007) Dissecting complex transcriptional responses using pathway-level scores based on prior information. *BMC Bioinformatics*, **8** (Suppl. 6), 1–7.
31. McKee, A.E., Neretti, N., Carvalho, L.E., Meyer, C.A., Fox, E.A., Brodsky, A.S. and Silver, P.A. (2007) Exon expression profiling reveals stimulus-mediated exon use in neural cells. *Genome Biol.*, **8**, R159.
32. Hang, X., Li, P., Li, Z., Qu, W., Yu, Y., Li, H., Shen, Z., Zheng, H., Gao, Y., Wu, Y. *et al.* (2009) Transcription and splicing regulation in human umbilical vein endothelial cells under hypoxic stress conditions by exon array. *BMC Genomics*, **10**, 126.
33. Mishra, M., Paunesku, T., Woloschak, G.E., Siddique, T., Zhu, L.J., Lin, S., Greco, K. and Bigio, E.H. (2007) Gene expression analysis of frontotemporal lobar degeneration of the motor neuron disease type with ubiquitinated inclusions. *Acta Neuropathol.*, **114**, 81–94.
34. Lin, C.L., Bristol, L.A., Jin, L., Dykes-Hoberg, M., Crawford, T., Clawson, L. and Rothstein, J.D. (1998) Aberrant RNA processing in a neurodegenerative disease: the cause for absent EAAT2, a glutamate transporter, in amyotrophic lateral sclerosis. *Neuron*, **20**, 589–602.
35. Flowers, J.M., Powell, J.F., Leigh, P.N., Andersen, P. and Shaw, C.E. (2001) Intron 7 retention and exon 9 skipping EAAT2 mRNA variants are not associated with amyotrophic lateral sclerosis. *Ann. Neurol.*, **49**, 643–649.
36. Gardina, P.J., Clark, T.A., Shimada, B., Staples, M.K., Yang, Q., Veitch, J., Schweitzer, A., Awad, T., Sugnet, C., Dee, S. *et al.* (2006) Alternative splicing and differential gene expression in colon cancer detected by a whole genome exon array. *BMC Genomics*, **7**, 325.
37. Kwan, T., Benovoy, D., Dias, C., Gurd, S., Serre, D., Zuzan, H., Clark, T.A., Schweitzer, A., Staples, M.K., Wang, H. *et al.* (2007) Heritability of alternative splicing in the human genome. *Genome Res.*, **17**, 1210–1218.
38. Hung, L.H., Heiner, M., Hui, J., Schreiner, S., Benes, V. and Bindereif, A. (2008) Diverse roles of hnRNP L in mammalian mRNA processing: a combined microarray and RNAi analysis. *RNA*, **14**, 284–296.
39. Di Giorgio, F.P., Carrasco, M.A., Siao, M.C., Maniatis, T. and Eggan, K. (2007) Non-cell autonomous effect of glia on motor neurons in an embryonic stem cell-based ALS model. *Nature Neuroscience*, **10**, 608–614.
40. Marchetto, M.C., Muotri, A.R., Mu, Y., Smith, A.M., Cezar, G.G. and Gage, F.H. (2008) Non-cell-autonomous effect of human SOD1 G37R astrocytes on motor neurons derived from human embryonic stem cells. *Cell Stem Cell*, **3**, 649–657.
41. King, A.E., Dickson, T.C., Blizzard, C.A., Woodhouse, A., Foster, S.S., Chung, R.S. and Vickers, J.C. (2009) Neuron-glia interactions underlie ALS-like axonal cytoskeletal pathology. *Neurobiol. Aging*, doi:10.1016/j.neurobiolaging.2009.04.004.
42. Talbot, K. and Davies, K.E. (2008) Is good housekeeping the key to motor neuron survival? *Cell*, **133**, 572–574.
43. Ule, J. (2008) Ribonucleoprotein complexes in neurologic diseases. *Curr. Opin. Neurobiol.*, **18**, 516–523.
44. Zhang, D., Paley, A.J. and Childs, G. (1998) The transcriptional repressor ZFM1 interacts with and modulates the ability of EWS to activate transcription. *J. Biol. Chem.*, **273**, 18086–18091.
45. Yang, L., Embree, L.J., Tsai, S. and Hickstein, D.D. (1998) Oncoprotein TLS interacts with serine-arginine proteins involved in RNA splicing. *J. Biol. Chem.*, **273**, 27761–27764.
46. Mercado, P.A., Ayala, Y.M., Romano, M., Buratti, E. and Baralle, F.E. (2005) Depletion of TDP 43 overrides the need for exonic and intronic splicing enhancers in the human apoA-II gene. *Nucleic Acids Res.*, **33**, 6000–6010.
47. Buratti, E., Stuani, C., De Prato, G. and Baralle, F.E. (2007) SR protein-mediated inhibition of CFTR exon 9 inclusion: molecular

- characterization of the intronic splicing silencer. *Nucleic Acids Res.*, **35**, 4359–4368.
48. Hirose, G. (1996) Paraneoplastic neurologic syndromes. *Intern. Med.*, **35**, 925–929.
 49. Akamatsu, W., Okano, H.J., Osumi, N., Inoue, T., Nakamura, S., Sakakibara, S., Miura, M., Matsuo, N., Darnell, R.B. and Okano, H. (1999) Mammalian ELAV-like neuronal RNA-binding proteins HuB and HuC promote neuronal development in both the central and the peripheral nervous systems. *Proc. Natl Acad. Sci. USA*, **96**, 9885–9890.
 50. Li, X., Lu, L., Bush, D.J., Zhang, X., Zheng, L., Suswam, E.A. and King, P.H. (2009) Mutant copper-zinc superoxide dismutase associated with amyotrophic lateral sclerosis binds to adenine/uridine-rich stability elements in the vascular endothelial growth factor 3'-untranslated region. *J. Neurochem.*, **108**, 1032–1044.
 51. Henneke, M., Diekmann, S., Ohlenbusch, A., Kaiser, J., Engelbrecht, V., Kohlschütter, A., Krätzner, R., Madruga-Garrido, M., Mayer, M., Opitz, L. *et al.* (2009) RNASET2-deficient cystic leukoencephalopathy resembles congenital cytomegalovirus brain infection. *Nat. Genet.*, **41**, 773–775.
 52. Boutz, P.L., Stoilov, P., Li, Q., Lin, C.H., Chawla, G., Ostrow, K., Shiu, L., Ares, M. Jr and Black, D.L. (2007) A post-transcriptional regulatory switch in polypyrimidine tract-binding proteins reprograms alternative splicing in developing neurons. *Genes Dev.*, **21**, 1636–1652.
 53. Makeyev, E.V., Zhang, J., Carrasco, M.A. and Maniatis, T. (2007) The MicroRNA miR-124 promotes neuronal differentiation by triggering brain-specific alternative pre-mRNA splicing. *Mol. Cell*, **27**, 435–448.
 54. Cheung, H.C., Hai, T., Zhu, W., Baggerly, K.A., Tsavachidis, S., Krahe, R. and Cote, G.J. (2009) Splicing factors PTBP1 and PTBP2 promote proliferation and migration of glioma cell lines. *Brain*, **132**, 2277–2288.
 55. Zacchigna, S., Lambrechts, D. and Carmeliet, P. (2008) Neurovascular signaling defects in neurodegeneration. *Nat. Rev. Neurosci.*, **9**, 169–181.
 56. Nave, K.A. and Trapp, B.D. (2008) Axon-glia signaling and the glial support of axon function. *Annu. Rev. Neurosci.*, **31**, 535–561.
 57. Stritt, C., Stern, S., Harting, K., Manke, T., Sinske, D., Schwarz, H., Vingron, M., Nordheim, A. and Knöll, B. (2009) Paracrine control of oligodendrocyte differentiation by SRF-directed neuronal gene expression. *Nat. Neurosci.*, **12**, 418–427.
 58. Gibson, R.M., Craig, S.E., Heenan, L., Tournier, C. and Humphries, M.J. (2005) Activation of integrin alpha5beta1 delays apoptosis of Ntera2 neuronal cells. *Mol. Cell Neurosci.*, **28**, 588–598.
 59. Kosodo, Y. and Huttner, W.B. (2009) Basal process and cell divisions of neural progenitors in the developing brain. *Dev. Growth Differ.*, **51**, 251–261.
 60. Dityatev, A. and Fellin, T. (2009) Extracellular matrix in plasticity and epileptogenesis. *Neuron Glia Biol.*, **5**, 1–13.
 61. Cayre, M., Canoll, P. and Goldman, J.E. (2009) Cell migration in the normal and pathological postnatal mammalian brain. *Prog. Neurobiol.*, **88**, 41–63.
 62. Wolburg, H., Noell, S., Wolburg-Buchholz, K., Mack, A. and Fallier-Becker, P. (2009) Agrin, aquaporin-4, and astrocyte polarity as an important feature of the blood-brain barrier. *Neuroscientist*, **15**, 180–193.
 63. Agrawal, S., Anderson, P., Durbeej, M., van Rooijen, N., Ivars, F., Opendakker, G. and Sorokin, L.M. (2006) Dystroglycan is selectively cleaved at the parenchymal basement membrane at sites of leukocyte extravasation in experimental autoimmune encephalomyelitis. *J. Exp. Med.*, **203**, 1007–1019.
 64. Kaiser, M., Maletzki, I., Hülsmann, S., Holtmann, B., Schulz-Schaeffer, W., Kirchhoff, F., Bähr, M. and Neusch, C. (2006) Progressive loss of a glial potassium channel (KCNJ10) in the spinal cord of the SOD1 (G93A) transgenic mouse model of amyotrophic lateral sclerosis. *J. Neurochem.*, **99**, 900–912.
 65. Nicaise, C., Soyfoo, M.S., Authélet, M., De Decker, R., Bataveljic, D., Delporte, C. and Pochet, R. (2009) Aquaporin-4 overexpression in rat ALS model. *Anat. Rec. (Hoboken)*, **292**, 207–213.
 66. Zhong, Z., Deane, R., Ali, Z., Parisi, M., Shapovalov, Y., O'Banion, M.K., Stojanovic, K., Sagare, A., Boillee, S., Cleveland, D.W. and Zlokovic, B.V. (2008) ALS-causing SOD1 mutants generate vascular changes prior to motor neuron degeneration. *Nat. Neurosci.*, **11**, 420–422.
 67. Mizuno, H., Warita, H., Aoki, M. and Itoyama, Y. (2008) Accumulation of chondroitin sulfate proteoglycans in the microenvironment of spinal motor neurons in amyotrophic lateral sclerosis transgenic rats. *J. Neurosci. Res.*, **86**, 2512–2523.
 68. Vitellaro-Zuccarello, L., Bosisio, P., Mazzetti, S., Monti, C. and De Biasi, S. (2007) Differential expression of several molecules of the extracellular matrix in functionally and developmentally distinct regions of rat spinal cord. *Cell Tissue Res.*, **327**, 433–447.
 69. Suwan, K., Choocheep, K., Hatano, S., Kongtawelert, P., Kimata, K. and Watanabe, H. (2009) Versican/Pg-M assembles hyaluronan into extracellular matrix and inhibits CD44-mediated signaling toward premature senescence in embryonic fibroblasts. *J. Biol. Chem.*, **284**, 8596–8604.
 70. Wang, M.J., Kuo, J.S., Lee, W.W., Huang, H.Y., Chen, W.F. and Lin, S.Z. (2006) Translational event mediates differential production of tumor necrosis factor-alpha in hyaluronan-stimulated microglia and macrophages. *J. Neurochem.*, **97**, 857–871.
 71. Ravits, J. and La Spada, A. (2009) Motor phenotype heterogeneity, focality and spread: deconstructing motor neuron degeneration. *Neurology*, **73**, 805–811.
 72. Nagai, M., Re, D.B., Nagata, T., Chalazonitis, A., Jessell, T.M., Wichterle, H. and Przedborski, S. (2007) Astrocytes expressing ALS-linked mutated SOD1 release factors selectively toxic to motor neurons. *Nat. Neurosci.*, **10**, 615–622.
 73. Brooks, B.R. (1994) El Escorial World Federation of Neurology criteria for the diagnosis of amyotrophic lateral sclerosis. *J. Neurol. Sci.*, **124** (suppl.), 96–107.
 74. Boelen, M.J., te Meerman, G.J., Gibcus, J.H., Blokzijl, T., Boezen, H.M., Timens, W., Postma, D.S., Groen, H.J. and van den Berg, A. (2007) Microarray amplification bias: loss of 30% differentially expressed genes due to long probe—poly(A)-tail distances. *BMC Genomics*, **8**, 277–290.
 75. Schroeder, A., Mueller, O., Stocker, S., Salowsky, R., Leiber, M., Gassmann, M., Lightfoot, S., Menzel, W., Granzow, M. and Ragg, T. (2006) The RIN: an RNA integrity number for assigning integrity values to RNA measurements. *BMC Mol. Biol.*, **7**, 3.
 76. Bolstad, B.M., Collin, F., Brettschneider, J., Cope, L., Simpson, K., Irizarry, R. and Speed, T.P. (2005) Quality assessment of Affymetrix GeneChip data. In Gentleman, R. (ed), *Bioinformatics and Computational Biology Solutions Using R and Bioconductor*. Springer Science+Business Media, Inc., New York, chapter 3, pp. 33–48.